Planetary and Space Science 218 (2022) 105432

Contents lists available at ScienceDirect

Planetary and Space Science

journal homepage: www.elsevier.com/locate/pss

Removal of straylight from ExoMars NOMAD-UVIS observations

Jonathon P. Mason [a,*], Manish R. Patel [a,b], Mark R. Leese [a], Brijen G. Hathi [a], Yannick Willame [d], Ian R. Thomas [d], Michael J. Wolff [c], Cédric Depiesse [d], James A. Holmes [a], Graham Sellers [a], Charlotte Marriner [a], Bojan Ristic [d], Frank Daerden [d], Jose Juan Lopez-Moreno [e], Giancarlo Bellucci [f], Ann Carine Vandaele [d]

[a] School of Physical Sciences, The Open University, Walton Hall, Milton Keynes, UK
[b] Space Science and Technology Department, Science and Technology Facilities Council, Rutherford Appleton Laboratory, Oxfordshire, UK
[c] Space Science Institute, 4750 Walnut Street, Suite 205, Boulder, CO, 80301, UCB 564, USA
[d] Royal Belgian Institute for Space Aeronomy, BIRA-IASB, 3 Avenue Circulaire, 1180, Brussels, Belgium
[e] Instituto de Astrofisica de Andalucía/CSIC, Granada, Spain
[f] Istituto di Astrofisica e Planetologia Spaziali, INAF, Rome, Italy

ARTICLE INFO

Keywords:
Straylight removal
Ultraviolet–visible spectroscopy

ABSTRACT

We present an in-flight straylight removal method for the Ultraviolet and Visible Spectrometer (UVIS) channel of the Nadir and Occultation for Mars Discovery (NOMAD) instrument aboard the ExoMars Trace Gas Orbiter (TGO). The presence of a 'red-leak' straylight signal in the UVIS instrument was discovered post-launch in ground calibration measurements of spectral lamps; UVIS observations of lamps with negligible UV light emission (RS12) showed a significant signal at UV wavelengths. Subsequent analyses of nadir observations of the martian atmosphere revealed that at UV wavelengths the red-leak straylight was in excess of 300% of the true UV signal, jeopardising the primary science observations of the instrument (retrievals of atmospheric ozone). By modifying the UVIS readout method to obtain a region of interest around the illuminated region on the Charge-Coupled Device (CCD) detector, instead of a binned one-dimensional spectrum, and utilising straylight profiles derived from measurements of the RS12 calibration lamp we show that the majority of the straylight at UV wavelengths can be successfully removed for the nadir channel in a self-consistent manner. The corrected UVIS radiances are compared to coincident Mars Color Imager (MARCI) instrument observations with residuals between the two instruments generally remaining within 15%.

1. Introduction

The Nadir and Occultation for Mars Discovery (NOMAD) instrument is a three-channel spectrometer currently in orbit around Mars on the European Space Agency (ESA)/Roscosmos ExoMars Trace Gas Orbiter (TGO) spacecraft. Two of the NOMAD channels, Solar Occultation (SO) and Limb Nadir and Occultation (LNO) observe at infrared wavelengths between 2.3 and 4.3 μm (Neefs et al., 2015).

The third channel is the Ultraviolet and Visible Spectrometer (UVIS) which has dual front-end telescopic viewing optics with an optical selector mechanism that enables the single UVIS spectrometer to observe in both solar occultation and nadir viewing geometries. In both viewing modes UVIS observes the wavelength range 200–650 nm at a resolution <2 nm. A full description of the UVIS instrument can be found in (Patel et al., 2017) and the system optical performance is described in (Vandaele et al., 2015).

Post-launch analysis of the ground calibration data from the NOMAD instrument revealed that light from visible and near-infrared (NIR) wavelengths was present on the detector in the UV region (Depiesse et al., 2018). Subsequent analysis of nadir observations revealed the straylight to be more than 300% of the UV signal and resulted in Hartley band ozone absorption being unresolved, preventing the measurement of ozone, one of the primary science species of interest for UVIS. This 'red-leak' aspect of UVIS straylight has been shown to have two components; a primary source from the NIR at wavelengths >650 nm and a lesser, secondary, broadband component from visible wavelengths (Depiesse et al., 2018). In this paper we describe a technique developed at The Open University, U.K., for the removal of this straylight from the

* Corresponding author.
E-mail address: jon.mason@open.ac.uk (J.P. Mason).

https://doi.org/10.1016/j.pss.2022.105432
Received 5 October 2021; Received in revised form 23 December 2021; Accepted 28 January 2022
Available online 2 February 2022

UVIS channel using in-flight observations, enabling a recovery of the primary science goals of UVIS.

It should also be noted that previous publications either use occultation data (Patel et al., 2021; Khayat et al., 2021), which has been straylight corrected, or high-altitude limb scans (Gérard et al., 2020, 2021). The straylight for these types of measurements is significantly lower than for nadir and in the case of the limb emission observations straylight is not applicable since there is no long wavelength emission in those spectra and thus no straylight.

The UVIS spectrometer instrument details are described in Section 2. In Section 3 the nadir channel straylight correction is described and in Section 4 the corrected UVIS radiances are compared to radiances from the Mars Color Imager (MARCI) (Bell et al., 2009).

2. The UVIS spectrometer

The UVIS spectrometer utilises two telescopes, one for nadir and the other for occultation geometries, with the light from the telescopes fed into a selector mechanism via a fibre bundle (nadir) or a single fibre (occultation). The selector mechanism controls which source, nadir or occultation, is fed into the optical bench with an optical layout based on a Czerny–Turner optical configuration. The incoming light from the selected fibre is focused onto the diffraction grating by the primary collimating mirror. A second collimating mirror focuses the dispersed light from the grating onto the CCD detector.

2.1. CCD readout process

To assess the straylight distribution, it is useful to define two areas on the CCD: (1) the illuminated (light) region (LR) defined as the area on the detector exposed to the incident light, and (2) the non-illuminated (light) region (NLR) which defines the pixels above and below the LR. The LR is bounded by a steep gradient in the signal, going from the background signal level in the NLR to the higher LR incident light signal level over five to ten pixels (depending on the wavelength). The upper (lower) boundary of the LR was defined by first finding the uppermost (lowermost) peak in signal from the input fibres and then looking for the pixel above (below) this point where the gradient in the signal slope reverses. The point of reversal in the gradient indicates that the pixel is no longer on the bounding signal slope of the LR and in the noisier NLR region. We also define two spatial components of the straylight: (1) in-axis straylight, which is the straylight present in the LR, and (2) off-axis straylight which is the straylight observed in the NLR between the LR and the detector readout register.

The original operational approach for UVIS was to bin the CCD array columns during readout into a one-dimensional spectrum to minimise the data volume, since no spatial information is recoverable from the detector given the use of optical fibres between the telescopes and optical bench. However, binning in such a way would result in the straylight being included in the final signal with no way to decouple the true signal from the straylight. The nominal UVIS readout method was modified to obtain a region of interest (ROI), such that it included sufficient NLR pixels (>10) in each column above and below the LR region to allow direct quantification of the NLR straylight.

The readout process is demonstrated in Fig. 1 for the nadir channel) which shows a full frame image of the UVIS detector for a Mars nadir measurement. The region bounded by the dotted white line is the nominal ROI readout during a nadir measurement. The CCD rows up to the ROI are 'dumped', a process whereby the register clock voltage is kept high, and the image clocks are cycled, to rapidly move the measured charge in the ROI out of the LR towards the register, this 'dump' process takes approximately 0.0122 s for the 56 rows dumped in a nominal nadir observation ROI of 189 rows. Once the 'dump' process is complete the ROI of 189 rows is readout nominally and takes approximately 2 s. In nadir mode the UVIS integration times are typically set to either 5, 7, 10 or 20 s with shorter integration times used for smaller solar zenith angles to avoid saturation at visible wavelengths. While the readout is comparable in length to the shorter integration times used by UVIS at least half of the pixels in the LR are moved quickly away from the incident light during the dump process. The last pixel in the LR used in the generation of the UVIS spectra will therefore accumulate an additional 0.4 s at UV wavelengths and 0.8 s at 650 nm of signal compared to the first pixel in the LR at those wavelengths.

The presence of straylight means the final raw signal in a UVIS measurement is formed of three, time dependent, components: 1) The charge accumulated in the LR from the desired light source, 2) the charge accumulated from dark current (DC) and in-axis straylight in the LR and 3) charge accumulated during the read-out process (smearing effect), resulting in the addition of charge due to off-axis DC and straylight in the NLR. The removal of the DC and smearing effect is described in the companion paper (Willame et al., *in review*) and in the following sections we solely consider removal of the straylight component in the LR

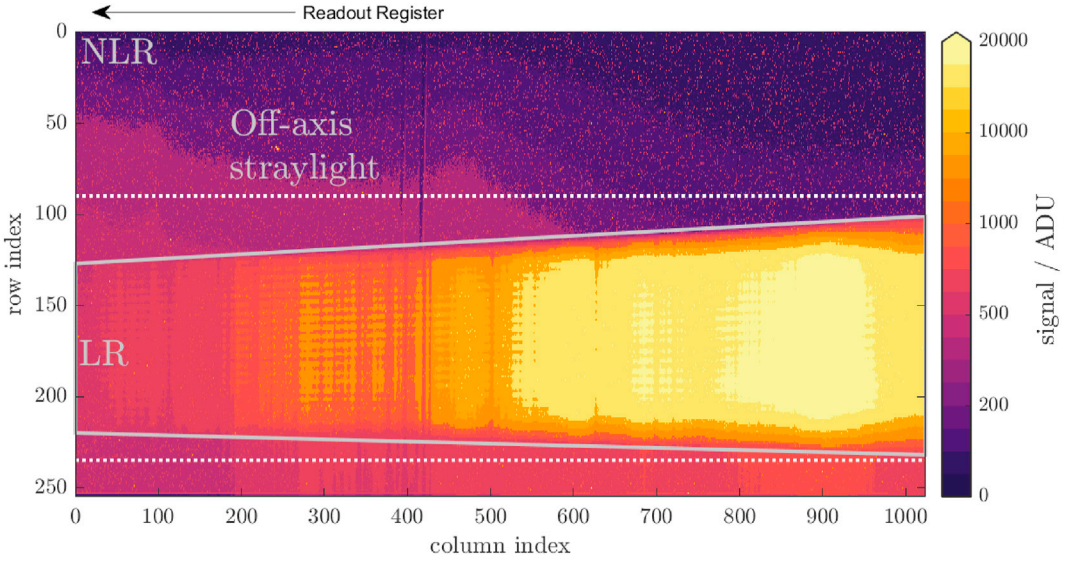

Fig. 1. Full frame image of the UVIS detector during a typical nadir measurement. The in-axis light dispersion is defined as the illuminated region (LR) and the off-axis area outside this region is defined as the non-illuminated region (NLR). The off-axis straylight can be seen between the LR and the detector readout register and the white dotted lines show the typical ROI of the CCD that is read out. The visible stratified lines seen in the LR is the illumination from the individual fibres.

introduced by the incident light source. The cause of the straylight within the UVIS optical system remains unknown and is the subject of continued analysis.

3. Nadir straylight correction

The correction method described in this section are independent of the source of straylight and utilise the off-axis straylight in the NLR to estimate the in-axis straylight in the LR in each individual observation, providing a self-consistent solution for each observation. An assumption is made that the ratio of the straylight in the NLR to the LR is constant and independent of the incident light source. Different methods are applied to the UV and visible wavelength regions because of limited measurements with no visible light incident on the UVIS detector taken prior to launch, meaning the straylight profiles could not be obtained.

3.1. Straylight removal procedure

Ground calibration measurements included the use of an RS12 lamp (Gamma scientific: RS12-DN HL1847) that had negligible emission <380 nm and, fortuitously, provided the opportunity to record the straylight in the UV region and from these measurements we derived a set of straylight profiles. Fig. 2 shows the raw output from one such RS12 lamp measurement and shows the straylight within the LR at wavelengths <380 nm (CCD column index <400). A peak in straylight is observed around column index 100, which unfortunately correspondents to wavelengths 238–258 nm, i.e. within the centre of the ozone absorption band which is a primary science target species for UVIS.

The CCD frame output from the RS12 lamp observation provides the ability to map straylight profiles across the UV region of the detector per CCD column as a function of CCD row. A moving average over five pixels was applied to the straylight profiles in each CCD column to obtain a smooth representation of the straylight behaviour. The smoothed straylight profiles for every fifth CCD column between column index 56 and 216, equating to a wavelength increment of ~2.3 nm and from 225 to 300 nm, are shown in Fig. 3. The fitted straylight profiles are normalised to unity to the first pixel read from the RS12 frame which is row index 107 in the full UVIS frame prior to the straylight correction procedure.

The correction procedure at UV wavelengths can be summarised in the following steps for each CCD column:

(1) Map the straylight profile row indices onto the measured row indices. A larger ROI is read out during inflight operations compared to ground calibration, to ensure sufficient pixels either side of the LR are measured. To correlate the row indices between inflight and calibration measurements we apply the formula for the ith pixel, $p_{s,i} = p_{m,i} + (p_{m,i_0} - p_{s,i_0})$ where p_{s,i_0} is the first pixel read in the straylight profiles and p_{m,i_0} is the first pixel read in the measured spectrum.
(2) Extract the NLR pixels above below the defined LR for both the measured spectrum and the straylight profile. Any anomalous pixel (i.e. hot pixel) is removed from both profiles.
(3) The straylight profile is scaled to the current measurement using the scaling factor, S, which is calculated by dividing the mean pixel value in the measurement NLR by the mean values of the NLR in the straylight profile.
(4) Scale the full straylight profile by S to obtain a straylight profile tailored to the specific observation and subtract the resultant profile from the measured column.

Fig. 4a shows an example of the correction procedure applied to a Mars observation at 250 nm. The final corrected UV signal is ~1000 ADU pixel^{-1} in the LR compared to a pre-corrected signal of ~5000 ADU pixel^{-1}, making the 'true' UV signal approximately one fifth of the measured raw signal in this example. It should be noted that not all the removed signal is a result of straylight in the LR, with other sources being in-axis DC, readout accumulation of off-axis DC and straylight.

The RS12 straylight profiles have only been directly measured in isolation across the CCD column for pixels <380 (<375 nm). For pixels between 381 and 719 (375 nm and 525 nm) a similar method, to the UV region, is used with the exception that the straylight profiles are derived from calibration measurements of a Tungsten Lamp (Osram Sylvania® model T6). From pixel 720 to 1024 (526 nm–654 nm) a second order polynomial is fitted between the NLR pixels above and below the LR as shown in Fig. 4b for 550 nm.

The straylight correction procedure relies on the assumption at the ratio of the straylight in the NLR to that in the LR, for a given wavelength, is independent of the incident light source and input flux. While we lack the means to rigorously test this assumption, since the straylight profiles can only be derived from a single light source during calibration, we can investigate whether the wavelength structure of the straylight changes inflight with different input fluxes, integration time and also whether it has been stable over the course of the UVIS science mission. Fig. 5 shows

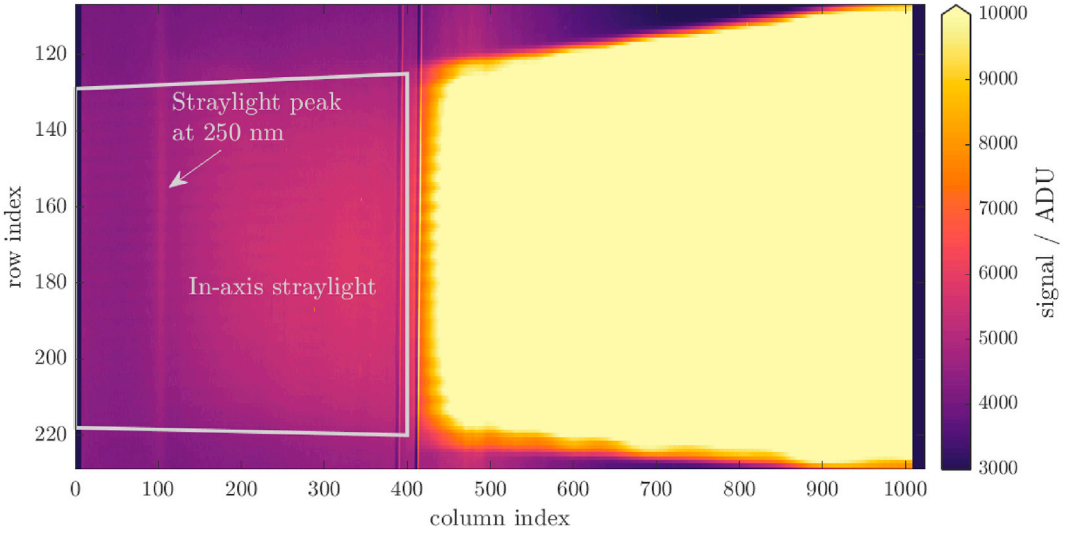

Fig. 2. UVIS detector observation of the RS12 lamp during the ground calibration campaign. Straylight is clearly observable at wavelengths <380 nm (column pixel 400) where there should be no emission by the RS12 lamp. The two lines visible in the UVIS image, around column pixel 400, is the dichotomy in the second order filter transmission profile (Patel et al., 2017).

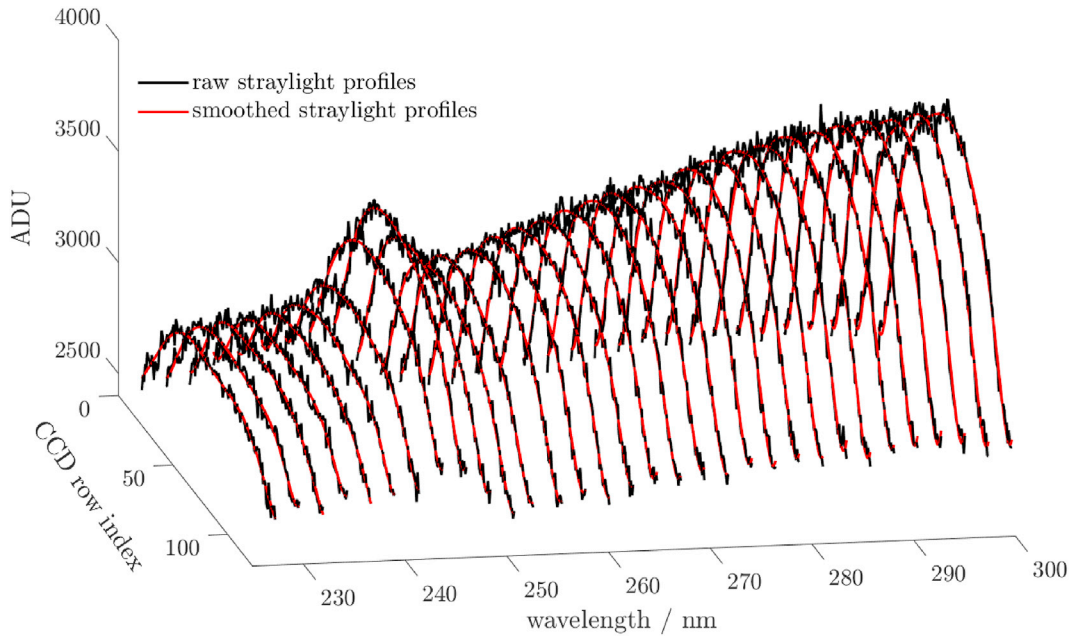

Fig. 3. The raw and fitted straylight profiles for wavelengths between 225 nm and 300 nm are shown in 2.3 nm steps (every 5 CCD columns) for clarity.

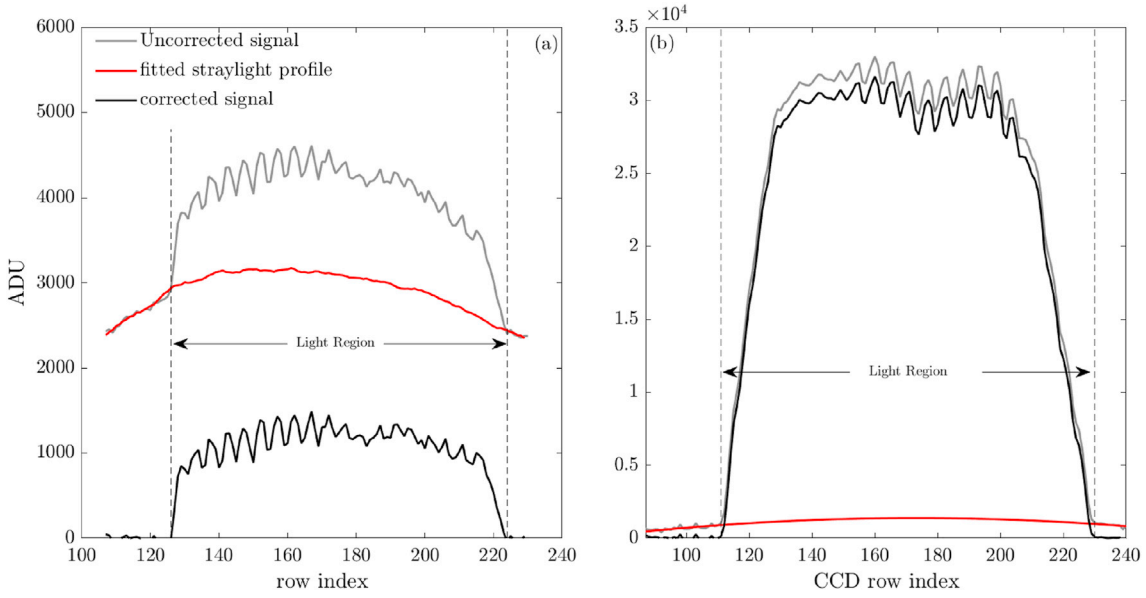

Fig. 4. Straylight fit at (a) 250 nm and (b) 550 nm for a nadir observation taken on 04 April 2018 at 00:40:52 (UTC).

the normalised wavelength dependent structure of the straylight at pixel position $(p_{m,i_0} - p_{s,i_0})$ in the NLR for a range of nadir observations covering different, solar zenith angles and locations to enable investigation into the dependence of the straylight structure on different input fluxes, integration times to confirm that the inflight straylight is independent of the exposure time and finally over the different martian seasons in Mars Year (MY) 34 and MY 35 to confirm that the straylight is stable over time. The straylight structure for each observation has been normalised to the mean of itself across all wavelengths to allow for a direct comparison of the straylight structure. The straylight structure shows the same peak in straylight near 250 nm, equivalent to the straylight peak observed in the RS12 lamp measurement. A secondary peak is also seen at around 410 nm; however, it is not clear whether this is straylight or introduce by the dichotomy in the second order filter transmission (Patel et al., 2017). More importantly, no clear variation is seen in the inflight straylight structure across the observations shown, indicating that the straylight structure in the wavelength dimension is independent of the incident flux and integration time. The fact the no change in the straylight structure is observed over time also provides evidence that the straylight is at least consistent and stable over all UVIS spectra and therefore the use of a constant NLR to LR straylight ratio is, at the very least, qualitatively justified.

3.2. Straylight application

The straylight procedure was applied to an entire UVIS dayside orbit (orbit file 20180424_072536) executed on 24 April 2018 between 07:25:36 and 08:35:15 UTC, corresponding to a solar longitude (L_s) of 164° in MY34. This orbit was selected because according to seasonal ozone results from the SPICAM instrument for MY27 (Perrier et al., 2006), the UVIS observations should experience regions of both low and high ozone abundances along its ground track. The spatial distribution of

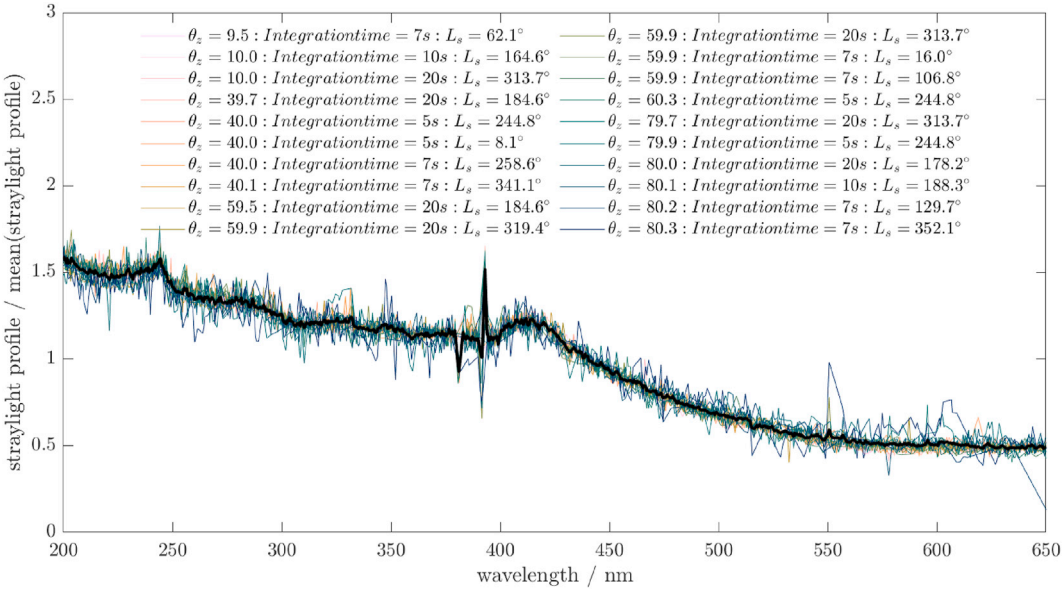

Fig. 5. The inflight straylight profile as a function of wavelength at pixel position ($p_{m,i_0} - p_{s,i_0}$) in the NLR for different, solar zenith angles, location, integration times and time of year. Each straylight profile has been normalised to the mean of itself across all wavelengths to emphasise that the straylight is independent of the incident flux, integration time and has been stable over the course of the UVIS science mission. The mean straylight structure as a function wavelength is shown by the black line.

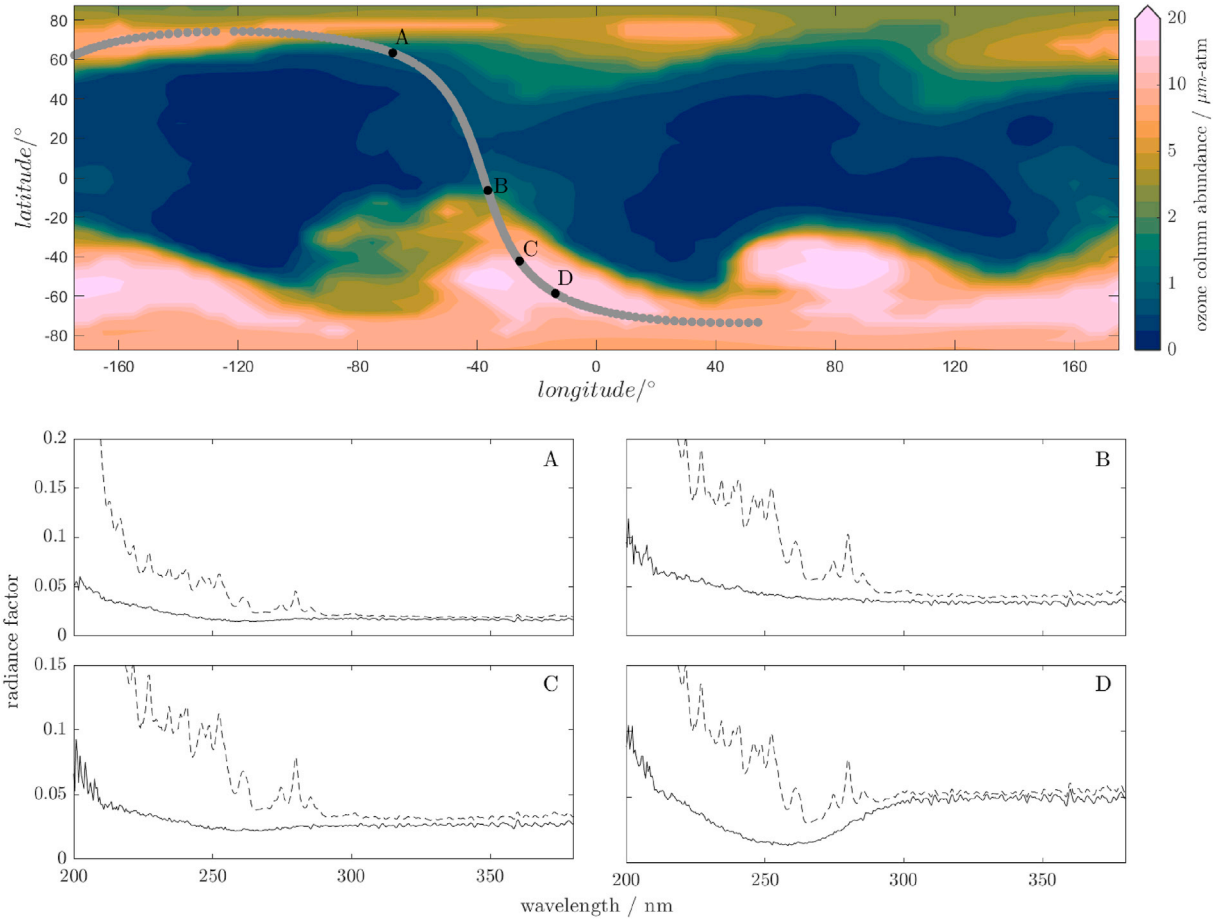

Fig. 6. The modelled distribution of ozone from the assimilation of SPICAM ozone column data (Holmes et al., 2018) for MY27 at $L_s = 164°$ with the UVIS ground track overlayed. The black points along the ground track correspond to the radiance factors shown in panel plots A-D for uncorrected UVIS data (dashed) and straylight removed data (solid).

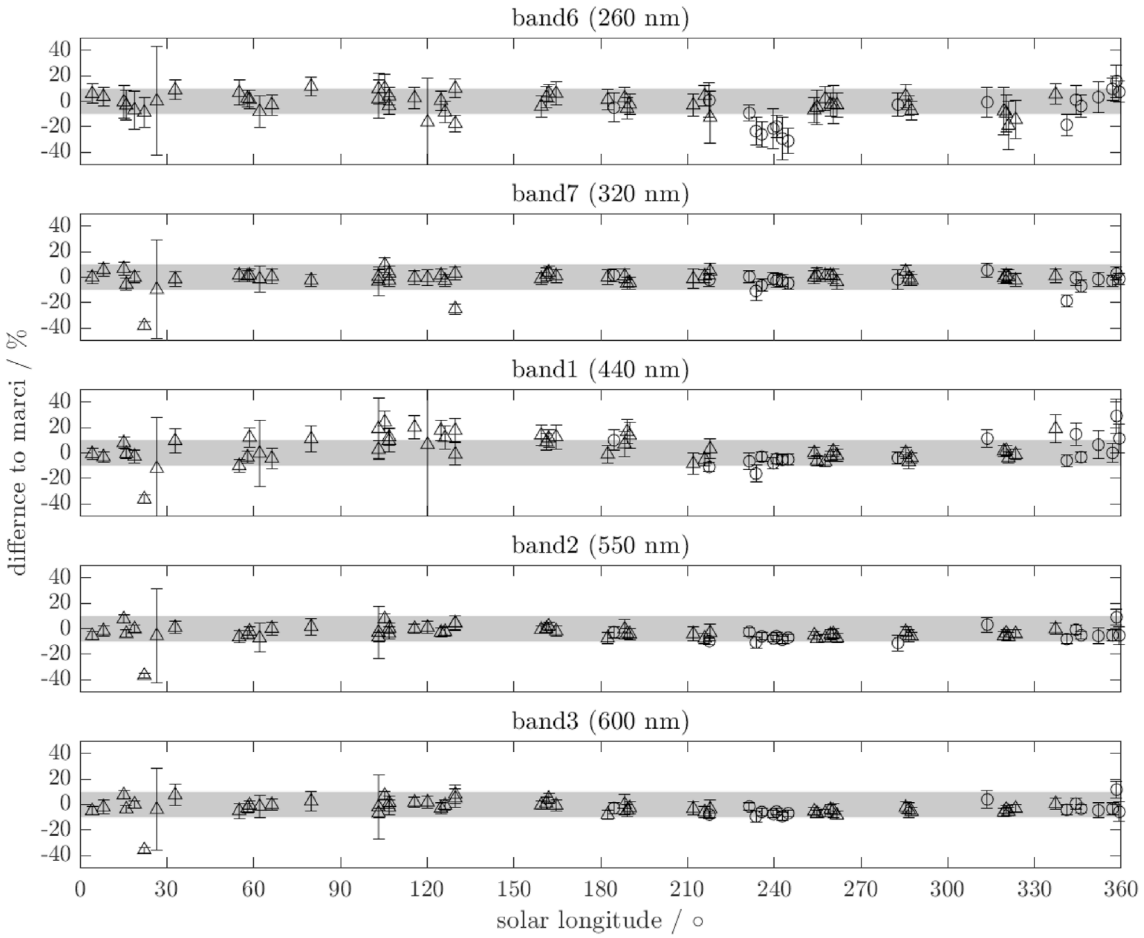

Fig. 7. The percentage difference in radiances from corrected UVIS and MARCI observations in MY34 (circles) and MY35 (triangles) that occur within 5 min and have a spatial separation of less than 1°. The grey shading defined the envelope of the ±10% difference range.

ozone shown in Fig. 6 is at the same time of year as the selected UVIS orbit but for MY27, derived from assimilation of SPICAM ozone column abundances into a Mars Global Circulation Model (Holmes et al. 2018, 2020). The displayed reanalysis output forms part of the Open access to Mars Assimilated Remote Soundings (OpenMARS) dataset, a reference dataset of the surface/atmospheric properties for almost nine Mars Years (Holmes et al., 2020). The calibrated radiance factor, before and after the straylight removal, for UVIS observations at points A-D are shown in the associated panel plots of Fig. 6. The effect of the straylight is immediately obvious and is the cause of the unphysical increase in the radiance at shorter wavelengths. The straylight removed spectra, on the other hand, shows the expected gradual increase in radiance factor at wavelengths <320 nm due to Rayleigh scattering. More importantly, the presence of ozone absorption (a broad absorption band centred around 250 nm) is observable in the corrected UVIS spectra at locations A, C, and D where we would expect to see ozone. Natural variability in the ozone could explain why C exhibits low ozone absorption compared to the MY27 assimilation at this time.

While this analysis is qualitative, it provides strong evidence that the majority of the straylight has been successfully removed from the UVIS channel at UV wavelengths with the ozone absorption band clearly resolvable in the corrected spectra. While it is not possible to ascribe a percentage to the amount of remaining straylight, we provide a comparison between UVIS radiances to that of MARCI in Section 4 to demonstrate the validity of the straylight removal approach.

4. UVIS-MARCI nadir comparison

To test the validity of the straylight removal method described in Section 3, we compared coincident observations by UVIS and the Mars Colour Imager (MARCI) instrument aboard the Mars Reconnaissance Orbiter (MRO) over the period May 2018–December 2020. MARCI is a multispectral imaging camera (Bell III et al., 2009) with seven filters centred at, 258, 320, 437, 546, 604, 653 and 718 nm, five of which are within the UVIS spectral range of 200–650 nm. The radiometric uncertainty for MARCI is ≤ 10% (Bell III et al., 2009; Wolff et al., 2010) making it an excellent choice to assess the viability and accuracy of the straylight removal technique described in Section 3. To make a like for like comparison, the UVIS data were convolved with the MARCI point spread function for the MARCI wavelengths: 263, 321, 440, 500 and 600 nm. A description and the calibration of the MARCI instrument, along with its radiometric uncertainty, can be found in (Bell III et al., 2009). The aim was to have, as near as possible, measurements by both instruments at the same time and location. To select appropriate observations for the comparison the following criteria were applied: solar incidence angle <75°, the angle between UVIS and MARCI < 2° and the UVIS and MARCI projection of the field of view on the surface of Mars <60 km. The footprints of the two instruments are different; UVIS has a curved rectangular footprint with a diameter of ~5 km and length between 20 and 100 km depending on the exposure time used, whereas, MARCI nadir observations produce a footprint of ~11 km by 720 km framelets, for each colour band, per frame acquisition (Bell III et al., 2009). To obtain radiances from MARCI the pixels that overlap with the UVIS footprint were averaged. It should be noted, however, that fractions of pixels are not considered here, and only full pixels are averaged even if part of a pixel is outside the UVIS ground track.

A comparison of all the coincident corrected UVIS and MARCI radiances are given in Fig. 7 which shows the difference between all the UVIS

and MARCI coincident observations that satisfy the set criteria; a total of 67 observations. The uncertainty shown for each observation in Fig. 7 is the UVIS error (Willame et al., 2022) added in quadrature with the standard deviation over all pixels in the MARCI observation. In all MARCI bands there is general agreement between the two instruments with 83% of the overlaps, for MARCI band 6, showing UVIS radiances within 15% of the MARCI radiances. Given the $\leq$10% radiometric uncertainty for MARCI, these results are in agreement within uncertainties and show the straylight correction, described in Section 3, can successfully remove the majority of the straylight from the UVIS nadir channel. The outlier observations were analysed but nothing abnormal in the processing was found and no correlation between the observations was found which could be attributed as the reason for the larger discrepancy with MARCI. The outliers may be attributed to the fact that only complete MARCI pixels are considered in this comparison and fractional pixel overlaps of MARCI pixels at the edge of the UVIS ground track are not considered. If a portion of one or more of these pixels transits over a region not observed by UVIS, for example a crater edge or ice surface that has a different surface albedo then it will cause a divergence of the radiances. Whether the radiance difference to MARCI is a result of imperfect removal of the straylight, observational difference or changes in the ozone column between the UVIS and MARCI observations is impossible to decouple. The fact that the outliers around Ls $= 240^{\circ}$ are only seen in the 260 nm band suggests a difference in the observed ozone column between the two measurements and not a result of imperfect straylight removal.

The agreement with MARCI is consistent throughout both MY34 and MY35 of UVIS operations and provides validation that the straylight is successfully removed from the raw data. More importantly, the detection of ozone absorption has been recovered and allows for fulfilment of the UVIS primary science objective.

5. Conclusion

We have shown that by utilising a ROI on the UVIS CCD detector to define the spread of straylight in the vertical dimension of the detector and application of straylight profiles derived from RS12 lamp ROI measurements, the straylight that is observed at UV wavelengths in the UVIS nadir channel can be successfully removed with corrected spectra revealing ozone absorption within the Hartley band. By using polynomial and linear fits between pixels, above and below the detector illuminated region, the majority of the straylight can be removed from the UVIS visible wavelengths. A comparison between UVIS and MARCI radiances for coincident observations provides validation of successful straylight removal with differences that are generally within $\pm$15% at all wavelengths.

This novel approach to straylight removal has resulted in the recovery of the UVIS main science objective, the mapping of atmospheric ozone in the martian atmosphere, and can potentially be applied to other similar spaceflight instruments to reduce straylight contamination, if present.

Author statement

The contribution of each author is given below using relevant Credit roles.

Jon Mason: Data curation, Investigation, Conceptualization, Methodology, Software, Formal analysis, Visualization, Writing - original draft **Manish Patel**: Data curation, Conceptualization, Investigation, Methodology, Supervision, Writing- Reviewing and Editing, Funding acquisition **Mark Leese**: Data curation, Methodology, Supervision **Brijen Hathi**: Data curation, Methodology, Formal analysis **Yannick Williame**: Data curation, Software, Formal analysis, Writing- Reviewing and Editing **Ian Thomas**: Project administration, Data curation, Writing- Reviewing and Editing **Michael Wolff**: Data curation, Validation, Writing- Reviewing and Editing **Cedric Depiesse**:: Data curation **James Holmes**: Data curation, Writing- Reviewing and Editing **Graham Sellers**: Validation, Writing- Reviewing and Editing **Charlotte Marriner**: Validation, Writing- Reviewing and Editing **Bojan Ristic**: Data curation **Frank Daerden**: Writing- Reviewing and Editing **Jose Lopez-Moreno**: Writing- Reviewing and Editing **Giancarlo Bellucci**: Writing- Reviewing and Editing **Ann-Carine Vandaele**: Project administration, Writing- Reviewing and Editing.

Declaration of competing interest

The authors declare that they have no known competing financial interests or personal relationships that could have appeared to influence the work reported in this paper.

Acknowledgements

The NOMAD experiment is led by the Royal Belgian Institute for Space Aeronomy (IASB-BIRA), with Co-PI teams in the United Kingdom (Open University), Spain (IAA-CSIC) and Italy (INAF-IAPS). This work was enabled through UK Space Agency grants ST/V002295/1, ST/V005332/1, ST/S00145X/1 and ST/R003025/1, and this project acknowledges funding by the Belgian Science Policy Office (BELSPO), with the financial and contractual coordination by the ESA Prodex Office (PEA 4000103401, 4000121493), by Spanish Ministry of Science and Innovation (MCIU) and by European funds under grants PGC2018-101836-B-I00 and ESP2017-87143-R (MINECO/FEDER), as well as by the Italian Space Agency through grant 2018-2-HH.0. This work was supported by the Belgian Fonds de la Recherche Scientifique – FNRS under grant number 30442502 (ET_HOME). The IAA/CSIC team acknowledges financial support from the State Agency for Research of the Spanish MCIU through the 'Center of Excellence Severo Ochoa' award for the Instituto de Astrofísica de Andalucía (SEV-2017-0709). US investigators were supported by the National Aeronautics and Space Administration.

References

Bell III, J.F., Wolff, M.J., Malin, M.C., Calvin, W.M., Cantor, B.A., Caplinger, M.A., Clancy, R.T., Edgett, K.S., Edwards, L.J., Fahle, J., Ghaemi, F., 2009. Mars reconnaissance orbiter Mars color imager (MARCI): instrument description, calibration, and performance. J. Geophys. Res.: Planets 114 (E8).

Depiesse, C., Willame, Y., Vandaele, A.C., Thomas, I.R., Bolsée, D., Neefs, E., Berkenbosch, S., Clairquin, R., Patel, M.R., Mason, J., Leese, M., 2018. September. Calibration of the NOMAD-UVIS channel. EPSC Meeting 12, EPSC2018, 2018.

Gérard, J.C., Aoki, S., Willame, Y., Gkouvelis, L., Depiesse, C., Thomas, I.R., Ristic, B., Vandaele, A.C., Daerden, F., Hubert, B., Mason, J., 2020. Detection of green line emission in the dayside atmosphere of Mars from NOMAD-TGO observations. Nat. Astron. 4 (11), 1049–1052.

Gérard, J.C., Aoki, S., Gkouvelis, L., Soret, L., Willame, Y., Thomas, I.R., Depiesse, C., Ristic, B., Vandaele, A.C., Hubert, B., Daerden, F., 2021. First observation of the oxygen 630 nm emission in the Martian dayglow. Geophys. Res. Lett. 48 (8) e2020GL092334.

Holmes, J.A., Lewis, S.R., Patel, M.R., Lefèvre, F., 2018. A reanalysis of ozone on Mars from assimilation of SPICAM observations. Icarus 302, 308–318.

Holmes, J.A., Lewis, S.R., Patel, M.R., 2020. OpenMARS: a global record of martian weather from 1999 to 2015. Planet. Space Sci. 188, 104962.

Khayat, A.S., Smith, M.D., Wolff, M., Daerden, F., Neary, L., Patel, M.R., Piccialli, A., Vandaele, A.C., Thomas, I., Ristic, B., Mason, J., 2021. ExoMars TGO/NOMAD-UVIS vertical profiles of ozone: 2. The high-altitude layers of atmospheric ozone. J. Geophys. Res.: Planets 126 (11) e2021JE006834.

Neefs, E., Vandaele, A.C., Drummond, R., Thomas, I.R., Berkenbosch, S., Clairquin, R., Delanoye, S., Ristic, B., Maes, J., Bonnewijn, S., Pieck, G., 2015. NOMAD spectrometer on the ExoMars trace gas orbiter mission: part 1—design, manufacturing and testing of the infrared channels. Appl. Opt. 54 (28), 8494–8520.

Patel, M.R., Antoine, P., Mason, J., Leese, M., Hathi, B., Stevens, A.H., Dawson, D., Gow, J., Ringrose, T., Holmes, J., Lewis, S.R., 2017. NOMAD spectrometer on the ExoMars trace gas orbiter mission: part 2—design, manufacturing, and testing of the ultraviolet and visible channel. Appl. Opt. 56 (10), 2771–2782.

Patel, M.R., Sellers, G., Mason, J.P., Holmes, J.A., Brown, M.A.J., Lewis, S.R., Rajendran, K., Streeter, P.M., Marriner, C., Hathi, B.G., Slade, D.J., 2021. ExoMars TGO/NOMAD-UVIS vertical profiles of ozone: Part 1–Seasonal variation and comparison to water. J. Geophys. Res.: Planets e2021JE006837.

Perrier, S., Bertaux, J.L., Lefèvre, F., Lebonnois, S., Korablev, O., Fedorova, A., Montmessin, F., 2006. Global distribution of total ozone on Mars from SPICAM/MEX UV measurements. J. Geophys. Res.: Planets 111 (E9).

Vandaele, A.C., Willame, Y., Depiesse, C., Thomas, I.R., Robert, S., Bolsée, D., Patel, M.R., Mason, J.P., Leese, M., Lesschaeve, S., Antoine, P., 2015. Optical and radiometric

models of the NOMAD instrument part I: the UVIS channel. Opt Express 23 (23), 30028–30042.
Wolff, M.J., Clancy, R.T., Goguen, J.D., Malin, M.C., Cantor, B.A., 2010. Ultraviolet dust aerosol properties as observed by MARCI. Icarus 208 (1), 143–155.
Willame, Y., Depiesse, C., Mason, J.P., Thomas, I.R., Patel, M.R., Hathi, B., Leese, M., Bolsee, D., Wolff, M.J., Trompet, L., Vandaele, A.C., Piccialli, A., Aoki, S., Ristic, B., Neefs, E., Beeckman, B., Berkenbosch, S., Clairquin, R., Mahieux, A., Pereira, N., Robert, S., Viscardy, S., Wilquet, V., Daerden, F., Lopez-Moreno, J.-J., Bellucci, G., 2022. Calibration of the NOMAD UVIS data in review.